

## Novel preparation of controlled porosity particle/fibre loaded scaffolds using a hybrid micro-fluidic and electrohydrodynamic technique

This content has been downloaded from IOPscience. Please scroll down to see the full text.

2014 Biofabrication 6 045010

(<http://iopscience.iop.org/1758-5090/6/4/045010>)

View [the table of contents for this issue](#), or go to the [journal homepage](#) for more

Download details:

IP Address: 144.82.107.79

This content was downloaded on 14/05/2015 at 13:25

Please note that [terms and conditions apply](#).

# Novel preparation of controlled porosity particle/fibre loaded scaffolds using a hybrid micro-fluidic and electrohydrodynamic technique

Maryam Parhizkar<sup>1</sup>, Panagiotis Sofokleous<sup>1</sup>, Eleanor Stride<sup>1,2</sup> and Mohan Edirisinghe<sup>1</sup>

<sup>1</sup> Department of Mechanical Engineering, University College London, Torrington Place, London, WC1E 7JE, UK

<sup>2</sup> Institute of Biomedical Engineering, Department of Engineering Science, Old Road Campus, University of Oxford, OX3 7DQ, UK

E-mail: [m.edirisinghe@ucl.ac.uk](mailto:m.edirisinghe@ucl.ac.uk)

Received 16 April 2014, revised 19 September 2014

Accepted for publication 24 October 2014

Published 27 November 2014

## Abstract

The purpose of this research was to produce multi-dimensional scaffolds containing biocompatible particles and fibres. To achieve this, two techniques were combined and used: T-Junction microfluidics and electrohydrodynamic (EHD) processing. The former was used to form layers of monodispersed bovine serum albumin (BSA) bubbles, which upon drying formed porous scaffolds. By altering the T-Junction processing parameters, bubbles with different diameters were produced and hence the scaffold porosity could be controlled. EHD processing was used to spray or spin poly(lactic-co-glycolic) (PLGA), polymethylsilsesquioxane (PMSQ) and collagen particles/fibres onto the scaffolds during their production and after drying. As a result, multifunctional BSA scaffolds with controlled porosity containing PLGA, PMSQ and collagen particles/fibres were obtained. Product morphology was studied by optical and scanning electron microscopy. These products have potential applications in many advanced biomedical, pharmaceutical and cosmetic fields e.g. bone regeneration, drug delivery, cosmetic cream lathers, facial scrubbing creams etc.

 Online supplementary data available from [stacks.iop.org/BF/6/045010/mmedia](http://stacks.iop.org/BF/6/045010/mmedia)

Keywords: electrohydrodynamic, microfluidic, scaffolds, microbubbles, particles, fibres, biomedical

(Some figures may appear in colour only in the online journal)

## 1. Introduction

Scaffolds play an important role in tissue engineering by acting as porous biodegradable structures containing various bio-

products (cells, genes, drugs and proteins) [1–4]. They serve as surrogate matrices, e. g. extra cellular (ECM) and can be produced from natural or synthetic material or a combination of both [5, 6]. In order for scaffolds to mimic the function of the natural ECM available in the human body, they must balance mechanical function with transport of bioactive agents [7, 8]. While a denser scaffold offers better function and mechanical strength, a more porous scaffold enables greater diffusion of gas/liquid components and promotes cell growth [6].



Content from this work may be used under the terms of the [Creative Commons Attribution 3.0 licence](http://creativecommons.org/licenses/by/3.0/). Any further distribution of this work must maintain attribution to the author(s) and the title of the work, journal citation and DOI.

Many techniques have been developed for the preparation of these porous matrices, including particle leaching [9], freeze drying [10], phase separation [11], electrospraying [12], and electrospinning [13] and recently bioprinting [14]. Scaffolds produced by these methods have pores with a wide size and shape distribution leading to insufficient transport of nutrition, migration and attachment of cells. Moreover, the use of organic solvents and particulate leaching in most of these techniques reduce the biocompatibility of the structure which hinders the growth of cells [15]. In order to create favourable scaffold environments the base material should have a suitable decomposition rate, good biocompatibility and surface characteristics and favourable plasticity [16]. Biodegradable materials from natural polymers such as hyaluronic acid, alginate and chitosan to synthetic polymers such as poly (L-lactic acid) (PLA) and poly (L-lactic-co-glycolic acid) (PLGA), are commonly used for the fabrication of scaffolds and have been extensively researched [17]. However, most polymeric scaffolds are hydrophobic and this discourages cell attachment and growth. In order to address this problem many methods have been suggested such as coating the scaffold with proteins or soaking it in various growth factors via spontaneous adsorption or covalent linking [18]. While these additional treatment methods assist with cell attachment and growth in polymeric matrices, they may also alter the morphological and physical properties of the scaffolds [19].

Recently bovine serum albumin (BSA) microbubbles have been used as porogens with low toxicity and high biocompatibility to fabricate scaffolds [20]. In addition to improvement in the porosity of scaffolds, albumin microbubbles can shield encapsulated growth factors from solvent denaturation. Nair *et al* [19] used a sonication technique to produce BSA microbubbles and fabricated scaffolds by phase separation of a polymer solution mixed with microbubbles. Microbubbles produced using the sonication technique generally have a wide size distribution and therefore the scaffolds produced with this method were not homogeneous. An alternative to this method is to use a microfluidic technique, whereby emulsions and foams characterized by monodisperse droplet/bubble sizes can be readily prepared. These systems could be used to generate porous materials with a highly consistent pore size [21, 22]. Microfluidic devices offer an unparalleled level of control over microbubble/droplet size and size distribution [23, 24]. Chiu *et al* [25] applied microfluidic techniques to generate gelatine microbubbles and incorporated them into scaffold structures in the microchannel. Colosi *et al* [26] used a microfluidic foaming technique for the generation of highly monodisperse gas-in-liquid poly(vinyl alcohol) (PVA) bubbles as a template for a scaffold characterized by an ordered and homogeneous porous texture.

In addition to microbubbles, particles containing growth factors have been incorporated into porous scaffolds [27]. Encapsulation of drugs into polymeric microparticles, and subsequent injection, is a proven method of controlled delivery for bioactive agents [28]. Electrohydrodynamic (EHD) processing can produce uniform solid and encapsulated particles and fibres with diameters ranging from a few

nanometres to several micrometres in a single step, under ambient conditions, at low cost and without the need for high concentrations of additives or surfactants [29, 30]. Moreover, multifunctional products (particles/fibres) loaded with therapeutic compounds (drugs, growth factors, DNA etc) can be generated via co-axial electrohydrodynamic processing (CEHD) [31]. However, there are limitations to incorporating polymeric particles/fibres into polymeric scaffolds due to the simultaneous equivalent solubility of the particles and scaffolds. Alternatively, protein-engineered biomaterials have the advantage of being able to combine desirable biocompatibility properties of natural ingredients with those of synthetic structures [32]. Proteins are complex organic macromolecules with an inhomogeneous charge distribution that results in amphiphilicity, structural flexibility and bioactivity, and therefore play a significant role in reinforcement, structuring and functionalization of ceramics and tissue engineering scaffolds [33, 34].

In this study we present a novel method that combines microfluidics with EHD processing to produce porous BSA scaffolds from microbubble templates with functional particles and/or fibres incorporated into the scaffolds' structure. The porosity and the size of the structures were controlled by adjusting the processing parameters of the microfluidic device. PLGA, PMSQ and collagen particles/fibres were then sprayed on them using the EHD technique. These secondary elements in the assembly of scaffolds can assist with the mechanical strength of the structure as well as providing a suitable route to deliver drugs and growth factors. The hybrid fabrication technique combines the high degree of control over size and size distribution offered by microfluidics to control pore size, with the efficiency of the electrospraying process for fibre generation. As with other electrohydrodynamic techniques it also offers excellent encapsulation efficiency for functional components, a low number of processing steps and the potential to apply the technique to a wide range of materials.

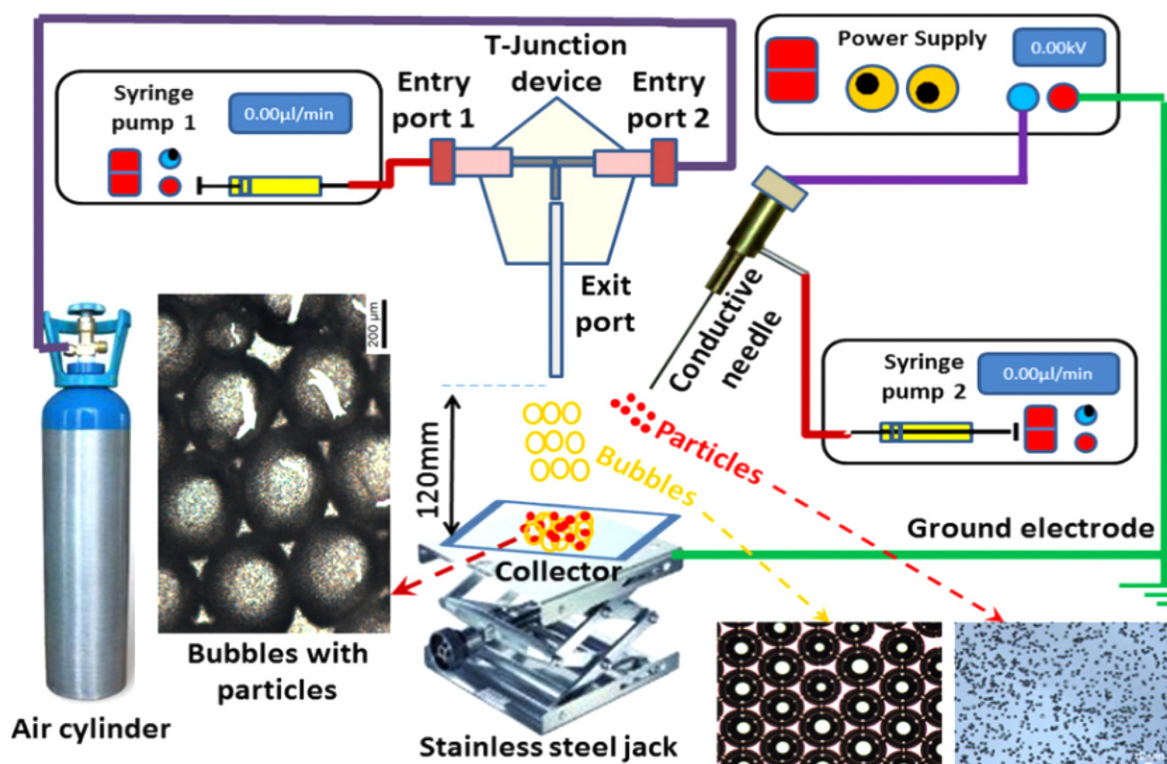
## 2. Materials and methods

### 2.1. Materials

Poly(lactic-co-glycolic) acid (PLGA co-polymer 50:50, Resomer RG503H, molecular weight:  $33000 \text{ g mol}^{-1}$ ) was purchased from Boehringer Ingelheim, (Ingelheim, Germany). Acetone, ethanol, collagen (Type I solution from rat tail in acetic acid), Tween 40, phosphate buffer saline (PBS), L- $\alpha$ -Phosphatidylcholine hydrogenated (phospholipid) and bovine serum albumin (BSA, molecular weight:  $66000 \text{ g mol}^{-1}$ ) were purchased from Sigma Aldrich (Poole, UK). Polymethylsilsesquioxane (PMSQ) with an average molecular weight of  $7465 \text{ g mol}^{-1}$  was obtained from Wacker Chemie AG, GmbH (Burghausen, Germany). Acetone and ethanol were used as solvents to prepare 5% w/w PLGA and 12% w/w PMSQ solutions, respectively, by dissolving them with magnetic stirrers in separate volumetric flasks until a homogenous suspension was formed. The collagen solutions

**Table 1.** Physical properties of liquids used in experiments. All % refer to weight unless stated otherwise.

Material or polymer solution	Density (kg m <sup>-3</sup> )	Viscosity (mPa s)	Surface tension (mN m <sup>-1</sup> )	Electrical conductivity (μS m <sup>-1</sup> )	pH
BSA 15%	1070 ± 20	1.62 ± 0.03	51.4 ± 0.1	6.44 ± 0.01 (x10 <sup>6</sup> )	6.71 ± 0.01
PLGA 5%	780 ± 10	0.78 ± 0.03	22.2 ± 0.2	339 ± 6	5.43 ± 0.06
PMSQ 12%	810 ± 10	1.04 ± 0.02	22.3 ± 0.2	730 ± 2	4.13 ± 0.06
Collagen 15% v/v	1060 ± 30	1.19 ± 0.02	51.6 ± 0.4	4.24 ± 0.02 (x10 <sup>6</sup> )	6.53 ± 0.02
Collagen 8% v/v	620 ± 20	0.76 ± 0.03	37.6 ± 0.4	3.62 ± 0.02 (x10 <sup>6</sup> )	5.64 ± 0.04

**Figure 1.** Schematic illustration of the T-Junction/EHD setup used for the experiments.

were prepared by adding the as received material into PBS solution and had a concentration of 8% and 15% v/v. Subsequently, the final solutions were vortexed for 120 s.

## 2.2. Characterization of solutions

The polymer solutions were characterized to determine their density, surface tension, viscosity, electrical conductivity and pH. Density was measured using a standard 25 ml density bottle. A Kruss tensiometer was used to measure the surface tension (standard Wilhelmy's plate method) and a U-Tube glass viscometer suitable for low viscosities (VWR International Ltd, Lutterworth, UK) was used to measure the viscosity of each solution. The electrical conductivity and pH of the solutions were determined using a Jenway 3540 pH/conductivity meter (Bibby Scientific Limited, Stone, UK). All the instruments were calibrated before use by following the manufacturers calibration guide and all experiments were performed at the ambient temperature of 25 °C, ambient pressure (101.3 kPa), and relative humidity (45–60%). Table 1 shows the measured liquids' physical properties used for the experiments.

## 2.3. Experimental setup

The experimental setup for producing the bubble/particle and bubble/fibre products is shown in figure 1. It consists of a single brass EHD needle device (inner diameter: 1.35 mm, outer diameter: 1.82 mm), a microfluidic T-Junction device (two entry ports and an exit port), two 'PhD 4400' high precision syringe pumps (Harvard Apparatus Limited, Edenbridge, UK) to control the flow rate of the solutions to one of the entry ports of the T-Junction device and to the EHD needle, a high precision voltage generator connected to the EHD needle (Glassman Europe Limited, Bramley, UK) and a gas supply cylinder, which transports air at high pressure into the secondary T-Junction entry port. Three fluorinated ethylene propylene (FEP) capillary tubes with internal diameter of 200 micrometre were inserted in a polydimethylsiloxane (PDMS) block to form the channels of the T-Junction set-up (more detail on the setup and schematic can be found in reference [35]). A 10 ml volume capacity Becton-Dickinson (Becton and Dickinson Company, Oxford, UK) syringe containing the 15% w/w BSA solutions was loaded to one of

the syringe pumps and a silicone tube was used to transfer it to one of the T-Junction entry ports. The other syringe pump was loaded with a 10 ml syringe filled with a different solution at each time (PLGA, PMSQ and collagen) and a silicone tube was used to transfer these to the EHD needle.

#### 2.4. Formation of bio-products

The processing conditions were optimised to form uniform and reproducible products in micro and nano scale dimensions, as described below:

(Video clips showing the different procedures used are included in the supplementary information provided.)

**2.4.1. Bubbles.** The T-Junction device was used to obtain the bubbles providing the scaffold template. Three different solutions of BSA 15% w/w were used to produce the bubbles: BSA, BSA + Tween 40 (90%/10%) and BSA + phospholipid solution (50%/50%). Air was used in all cases as the gas phase. Following bubble production, the most stable ones (assessing them by the number of bubbles bursting in time) before and after drying were chosen for the experiments. The bubble diameter was controlled by changing the air pressure and liquid flow infused to the T-Junction device. The processing conditions were optimised to generate monodispersed bubbles for each experiment. The working distance between the T-Junction needle tip and the collector (glass slide) was set to 120 mm. Once the bubbles were collected on glass slides, they were left to dry at ambient temperature and pressure.

**2.4.2. Particles.** The EHD process was used to produce polymeric particles. The processing conditions (flow rate, voltage) were optimised to form particles in nano and sub-micro scale in order to increase their density per mm<sup>2</sup> on the bubbles' surfaces. To achieve this, EHD parameters were optimised to obtain a stable cone-jet at the EHD needle tip [36, 37].

**2.4.2.1. PLGA.** To produce the PLGA particles the voltage was set to 11 kV and the flow rate of the PLGA solution was fixed at 20  $\mu\text{l min}^{-1}$ . The working distance between the needle tip and the collector (glass slide) was set to 120 mm and the distance between the EHD needle and the T-Junction tip was set at a distance of 50 mm. The EHD needle was set at an angle of 45° (Reference Angle (RA): At 0° if the EHD needle was set at a vertical position with its nozzle facing the ground) in order to spray directly onto the bubbles that were produced from the T-Junction process.

**2.4.2.2. PMSQ.** To produce the PMSQ particles the voltage was set to 9 kV and the flow rate of the PLGA solution was fixed at 10  $\mu\text{l min}^{-1}$ . All the other parameters remained the same as in the PLGA particles production experiment.

**2.4.2.3. Collagen.** Collagen solution 8% v/v was used to form the particles. The voltage was set to 14 kV and the flow rate of the collagen solution was fixed at 5  $\mu\text{l min}^{-1}$ . All the

other parameters remained the same as in previous experiments.

**2.4.3. Collagen beaded nanofibres.** To form collagen fibres, a solution of 15% v/v collagen was used and the applied voltage was set to 21 kV. The flow rate of the collagen solution was fixed at 3  $\mu\text{l min}^{-1}$ . All the other parameters remained the same as in the previous experiments. In this study beading was deliberately exploited as a means of increasing the volume of material into which a functional component can be incorporated.

#### 2.5. Combination of bio-products

After the production of the BSA bubbles two different experimental approaches were followed to spray the secondary bio-products onto the bubbles: a) when the bubbles were produced by the T-Junction process, the secondary bio-products formed by the EHD process were simultaneously sprayed directly on them (figures 1a and b) the bubbles/scaffolds were left to dry after their production and then the secondary bio-products were sprayed on them.

#### 2.6. Product characterization

The bubbles/scaffolds, particles, fibres and the combined structures were analysed for their diameter and surface morphology by optical microscopy (Micropublisher 3.3 RTV, 3.3 megapixel CCD Color-Bayer Mosaic, Real Time Viewing camera, MediaCybernetics, Marlow, UK) and scanning electron microscopy (Hitachi S-3400N and JEOL JSM-6301F field emission scanning electron microscopes, SEM). The bubbles, bubble/particle and bubble/fibre structures were collected and studied by optical microscopy immediately and after 15 and 30 min after production to detect any changes in their size and morphology. Then they were left to dry for 12 h and then studied by scanning electron microscopy at an acceleration voltage of 3–5 kV. All the samples were vacuum-coated with gold for 120 s before obtaining SEM images. Analysis of the products was carried out using the Image-Pro Insight software (MediaCybernetics Ltd, Marlow, UK).

### 3. Results and discussion

#### 3.1. Bubble formation

After the bubbles were produced they were monitored for their stability (number of bubbles bursting as time progressed and how long they need to dry in order to obtain a solid scaffold). The most stable bubbles were the BSA bubbles obtained without the addition of any surfactants or phospholipids. Hence the experiments were continued with the BSA solution only. It is well known that by adjusting the T-Junction processing parameters (solution concentration, gas pressure, liquid flow and capillary diameter size) bubbles of different size can be generated [35]. In this study, BSA bubbles ranging from ~80  $\mu\text{m}$  to ~550  $\mu\text{m}$  were produced by

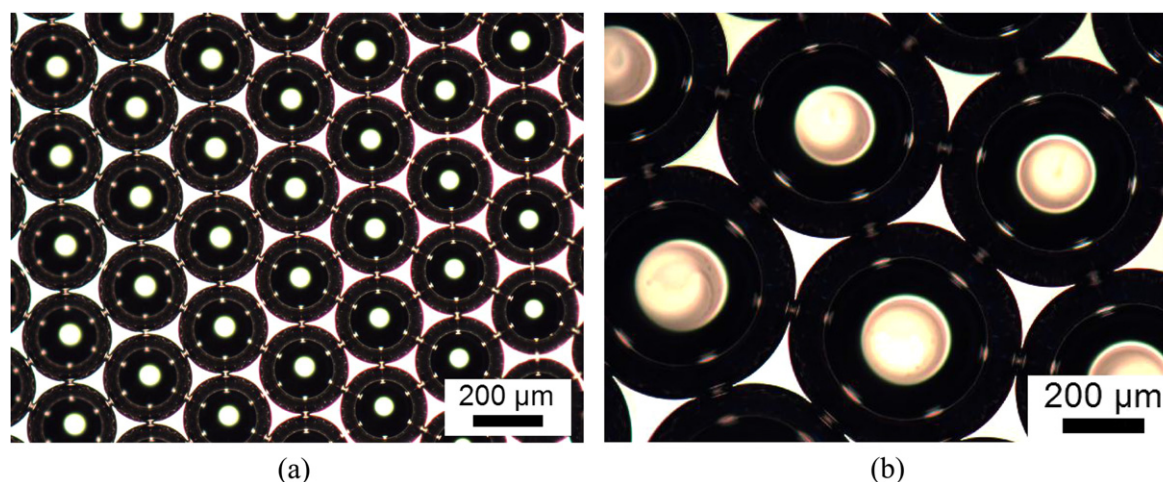


**Figure 2.** BSA bubbles produced from the T-Junction.

**Table 2.** Parameters used to generate bubbles and their stability. (The bubble-diameter value is the mean diameter of 50 bubbles.)

Solution	Air pressure (kPa)	Liquid flow ( $\mu\text{l min}^{-1}$ )	Bubble diameter ( $\mu\text{m}$ )	Stability
BSA	32.3	200	$81 \pm 2$	Stable until dried
	34.9	200	$95 \pm 2$	
	41.2	200	$141 \pm 3$	
	42.7	200	$152 \pm 4$	
	44.3	200	$162 \pm 3$	
	45	200	$164 \pm 3$	
	46.1	200	$174 \pm 4$	
	48.3	200	$190 \pm 4$	
	51.6	200	$208 \pm 4$	
	57.3	200	$251 \pm 2$	
	75	200	$302 \pm 2$	
BSA + Phospholipid	53	200	$245 \pm 5$	Unstable, burst prior to drying
	75	200	$285 \pm 5$	
BSA + Tween 40	1100	200	$82 \pm 4$	Unstable, burst prior to drying
	1200	200	$95 \pm 4$	

keeping the liquid flow rate constant at  $200 \mu\text{l min}^{-1}$ , while increasing the gas pressure from 30 to 100 kPa. Examples of the bubbles produced are shown in figure 2 with images (a) and (b) showing bubbles having an average diameter of  $251 \pm 2 \mu\text{m}$  and  $408 \pm 4 \mu\text{m}$ , respectively. Table 2 shows the parameters used to obtain the different bubble diameters.

### 3.2. Scaffold structure

The bubbles produced from the T-Junction process had a foam like texture, hence to produce the multi-layered BSA scaffolds the bubbles were left to dry for a short period of time (20 min–60 min) before being sprayed onto. Figure 3 shows the BSA bubbles immediately after generation and at different time intervals while drying. The bubbles in this case had an average size of  $81 \pm 2 \mu\text{m}$ .

**3.2.1. Single layer structure.** By collecting a single layer of BSA bubbles on a glass slide and leaving it to dry for 20 min

a single layer honeycomb arrangement with approximately the same diameter scaffold window was obtained. Figure 4 shows these structures with a(i) and b(i) having average window diameters of  $152 \pm 7 \mu\text{m}$  and  $208 \pm 8 \mu\text{m}$ , respectively and the images [(a, b)ii] showing the same structures at higher magnification. The depth of the windows was found to be  $100 \pm 9 \mu\text{m}$  almost  $\frac{1}{2}$  the pore diameter and the interconnected regions of the dried bubbles had an average thickness of  $30 \pm 9 \mu\text{m}$ .

**3.2.2. Double layer structure.** By changing the T-Junction parameters, the bubbles' size was increased and a two layered structure was obtained by adding another layer on the top of a single layer of bubbles instantly after collection on the glass slide. The structure was also left to dry for 20 min and after analysis it was found that the windows formed had an average diameter of  $190 \pm 8 \mu\text{m}$ . Figure 5 shows images of the two layered structure taken by optical microscope and SEM with figure 5(a) clearly showing the double layered arrangement.

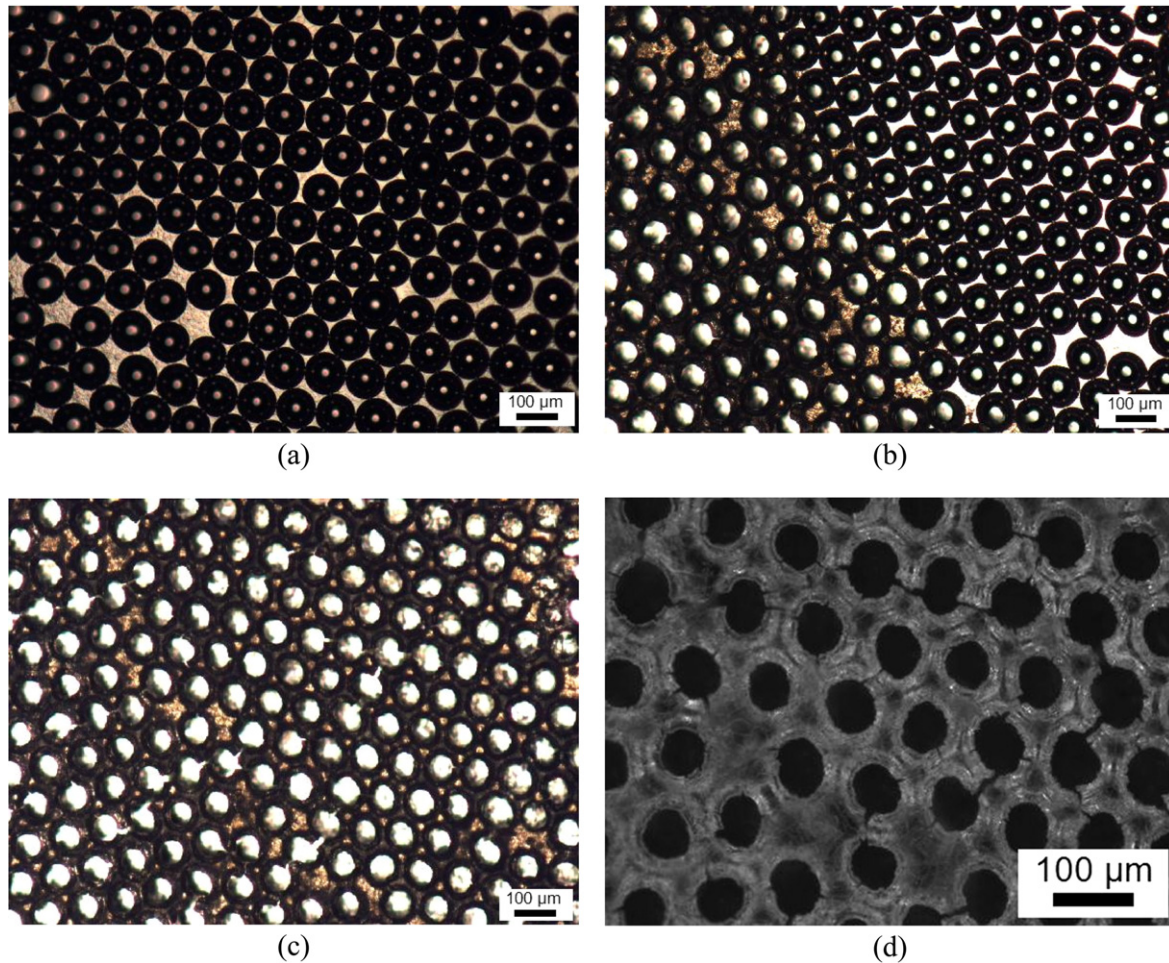


**Figure 3.** Optical microscope images of BSA bubbles: (a) 1 min, (b) 10 min, (c) 15 min and (d) 20 min after generation.

The thickness of the two layer structure formed had an average value of  $342 \pm 11 \mu\text{m}$ .

**3.2.3. Multilayer scaffold.** After experimenting with the single and double layered structures, scaffolds were formed by accumulating many layers of bubbles. By adjusting the T-Junction processing parameters, mainly increasing the gas pressure to control the bubble size and collecting multiple layers of bubbles on a glass slide or a glass vial, 3D scaffolds with different window sizes and hence porosity, were produced. The BSA bubbles spontaneously self-assembled into liquid foam structures, which were solidified after leaving to dry for 60 min. During the drying process, the pressure difference between the bubbles and the ambient atmosphere ruptured the film between the bubbles and only the plateau borders were left. The dried foam formed 3D scaffolds and by adjusting the T-Junction processing parameters four different structures were obtained with window diameters of  $162 \pm 17 \mu\text{m}$ ,  $327 \pm 24 \mu\text{m}$ ,  $478 \pm 28 \mu\text{m}$  and  $543 \pm 33 \mu\text{m}$  obtained at various gas pressures of 44, 67, 93 and 102 kPa, respectively. Figure 6 shows these scaffolds with figure 6(a) having the biggest pore size and figure 6(d) the smallest. The figures indicate the ordered and interconnected pores of the 3D scaffolds. It was noticed that

despite the monodispersity of the bubbles formed during the process the diameter size distribution of the scaffolds pores was broader in the multi-layered scaffolds than in the single and double layered structures obtained at the previous experiments. This can also be confirmed from the relatively large standard deviation values measured (17, 24, 28 and 33) during the scaffold pore size analysis. This was probably caused by the increased pressure due to the weight of the bubbles located on the top layers acting on the bubbles in the lower layers. However, the pore size of the scaffolds produced in this study with the T-Junction process still had a narrower size distribution than other techniques used to fabricate scaffolds. It was also noticed in some cases that when the BSA bubbles were bursting during the drying process a thin cracked layer of protein coating was left at the sides of the scaffolds gaps. According to Nair *et al* [19] this thin protein coating may serve as a biocompatible layer to promote cell seeding and growth.

### 3.3. Particles sprayed on bubbles

The first experimental approach was to spray the bio-particles formed by the EHD process onto the BSA bubbles generated via the T-Junction process simultaneously. In this procedure the stability of the bubbles was affected by the particles

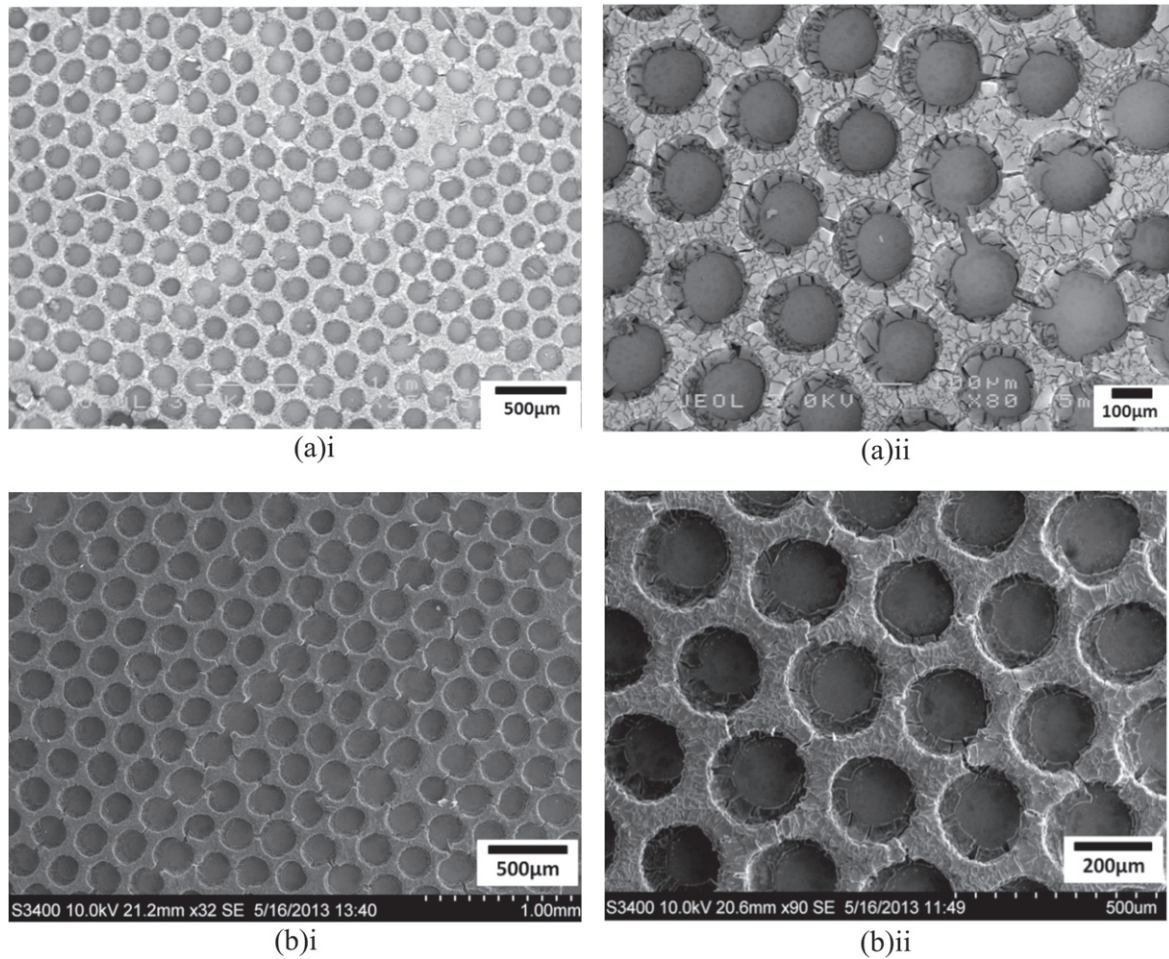


**Figure 4.** SEM images of a single layer of dried BSA bubbles formed on a glass slide with [(a,b)i] showing structures with two different window diameters controlled by changing the T-Junction parameters and [(a,b)ii] showing the images in [(a,b)i] at higher magnification.

accelerated due to the electric potential difference induced by the EHD process rupturing the bubbles shell and causing them to burst. Approximately 30% of the bubbles produced were bursting due to this effect. Although many strategies were attempted to resolve this, such as adjusting the liquid flow rate into the EHD needle, increasing the BSA concentration and the distance between the EHD needle tip and the collection area, none had a significant effect on the bubbles stability. An advantage of this approach, however, was that the particles were distributed equally in the inner and outer surfaces of the scaffold while it was formed.

The second experimental approach was to leave the scaffold to dry and then spray the particles onto it. The advantage of this method was that the bubbles were left to dry without any external disturbance and thus the percentage of bubbles bursting decreased to less than 5%. Also the particles were still able to infiltrate into the scaffolds' structure very easily because of their small size, and hence were distributed on the scaffolds' inner surfaces. As expected, however the outer surface of the final scaffold had a higher density of particles than the inner ones.

**3.3.1. PLGA particles.** The bubble and particle sizes used for this experiment were  $141 \pm 3 \mu\text{m}$  and  $130 \pm 23 \text{ nm}$  (mean

diameter of 100 particles), respectively. Firstly, PLGA particles were sprayed onto wet (not dried) bubbles (figures 7(a) and (b)) and then PLGA particles were sprayed onto a single layered (figure 7(c)), two layered (figure 7(e)) and multi layered (figure 7(f)) BSA scaffolds.

In order to check if the particles had infiltrated into the inner layers of the BSA scaffold, the surface of the structure was removed by a surgical blade. Figure 7(c) confirms that the particles were present on the bottom layer of the scaffold. Figure 7(d) shows the PLGA particles aggregating into different shapes while they were sprayed into the inner cavities of the scaffold. This is caused by the difference in the hydrophobic and hydrophilic nature of the PLGA and BSA, respectively [38, 39].

**3.3.2. PMSQ particles.** The average window diameter of the multilayered scaffold was measured and found to be  $95 \pm 41 \mu\text{m}$ . The PMSQ particles sprayed had an average size of  $1.94 \pm 0.4 \mu\text{m}$  (mean diameter of 100 particles). Figure 8 shows SEM images of the same BSA scaffold at different magnifications after being sprayed with PMSQ microparticles. It can be seen clearly that the particles

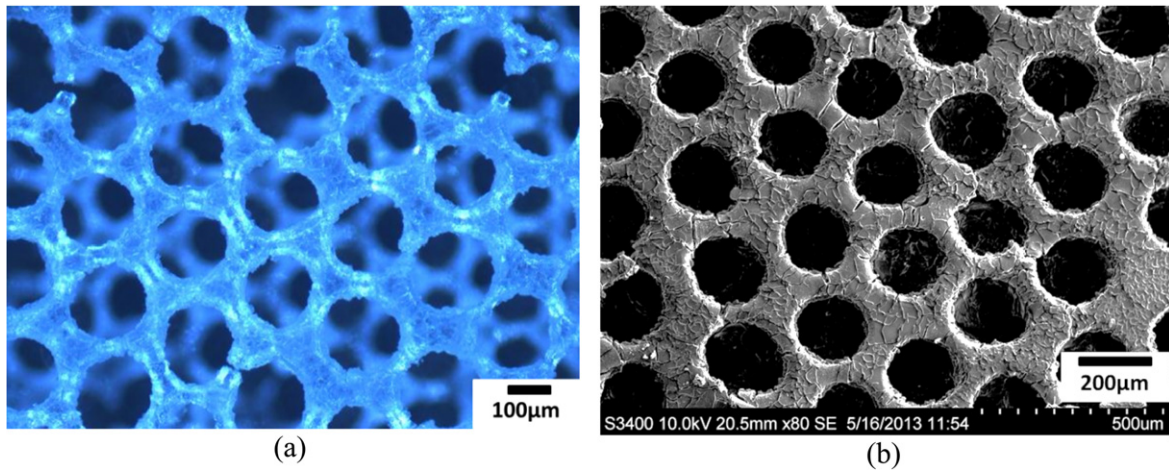


**Figure 5.** Double layer dried BSA scaffold structure (a) optical and (b) SEM micrographs.

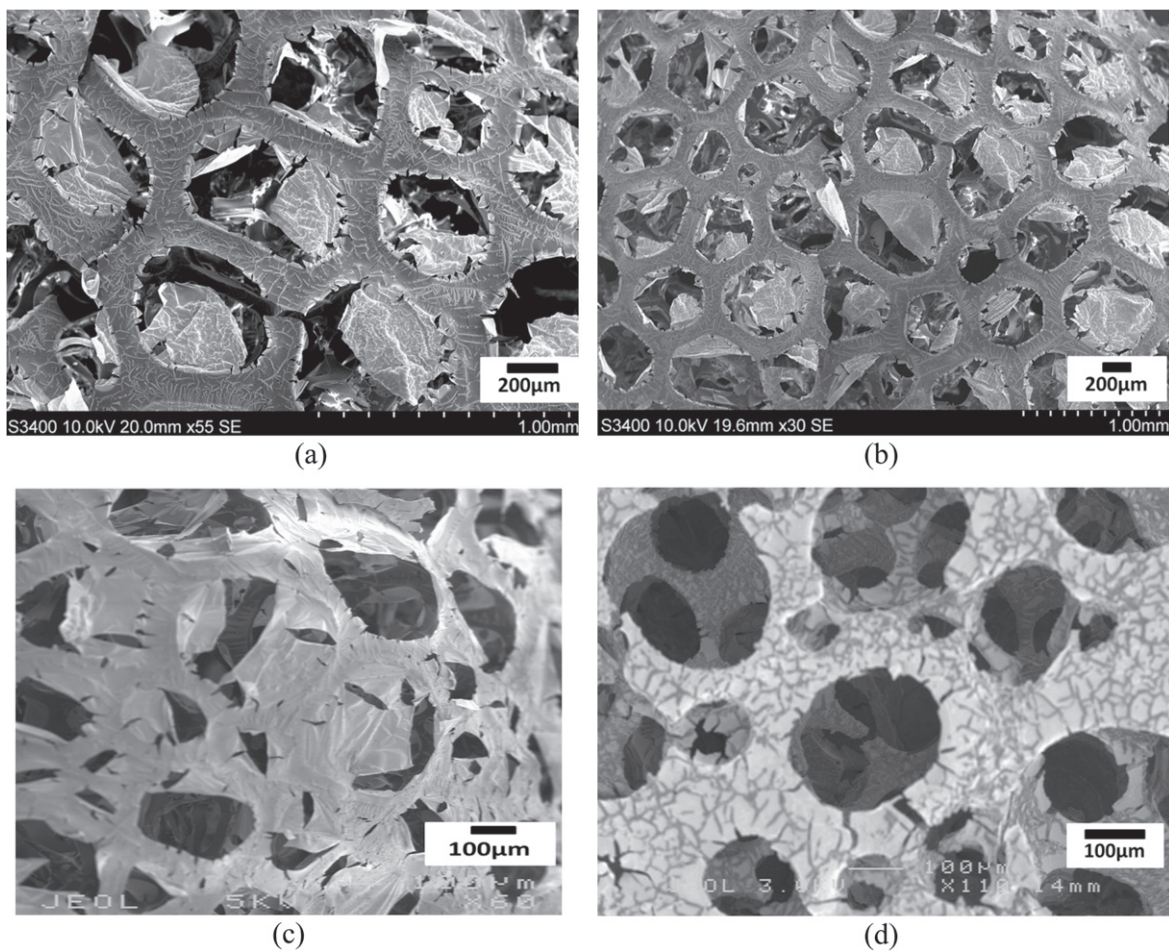


**Figure 6.** Scanning electron micrographs of multi-layer scaffolds made using dried BSA bubbles showing the different diameter window sizes obtained by changing the T-Junction processing parameters (a) having the biggest window diameter ( $543 \pm 33 \mu\text{m}$ ) and (d) the smallest one ( $162 \pm 17 \mu\text{m}$ ).

infiltrated the inner surfaces of the scaffold and were distributed homogeneously.

**3.3.3. Collagen particles.** In these experiments the pores of the scaffold prepared had an average diameter of  $174 \pm 8 \mu\text{m}$  and the collagen particles sprayed on it had a size of

$1.35 \pm 0.3 \mu\text{m}$  (mean diameter of 100 particles). Figure 9 shows SEM images at different magnifications of the same BSA scaffold sprayed with collagen micro-particles. It was observed that the scaffold surface (see figure 9(f)) appeared degraded due to spraying the collagen particles. This was caused by the low concentration of acetic acid found in the

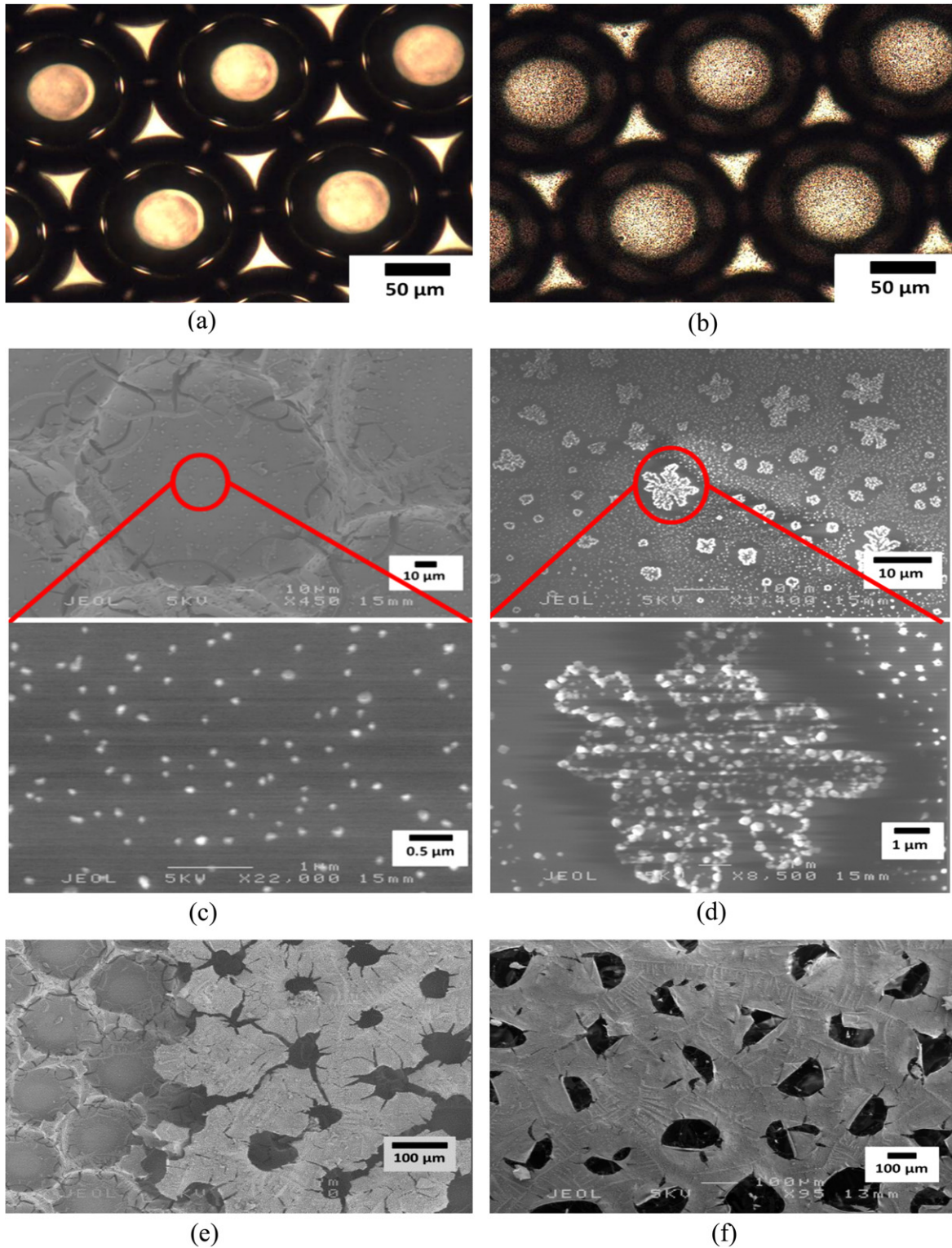


**Figure 7.** Images showing (a) dried BSA bubbles, (b) dried BSA bubbles with PLGA nanoparticles, (c) a single layer BSA scaffold with PLGA nanoparticles in its cavities after spraying for 1 min (see arrows), (d) PLGA nanoparticles aggregating into different shapes in a BSA scaffold cavity after spraying for 5 min (e) a two layer BSA scaffold with PLGA nanoparticles and (f) a multilayer BSA scaffold with PLGA nanoparticles.

collagen type I solution used for the experiments. When the collagen solution was sprayed onto the scaffold, it is assumed that the acid did not fully evaporate during the flight from the EHD needle tip to the collection area

(probably due to its high boiling point of 118 °C), hence causing the protein based surface of the scaffold to locally dissolve and the collagen particles to embed into the BSA scaffold.

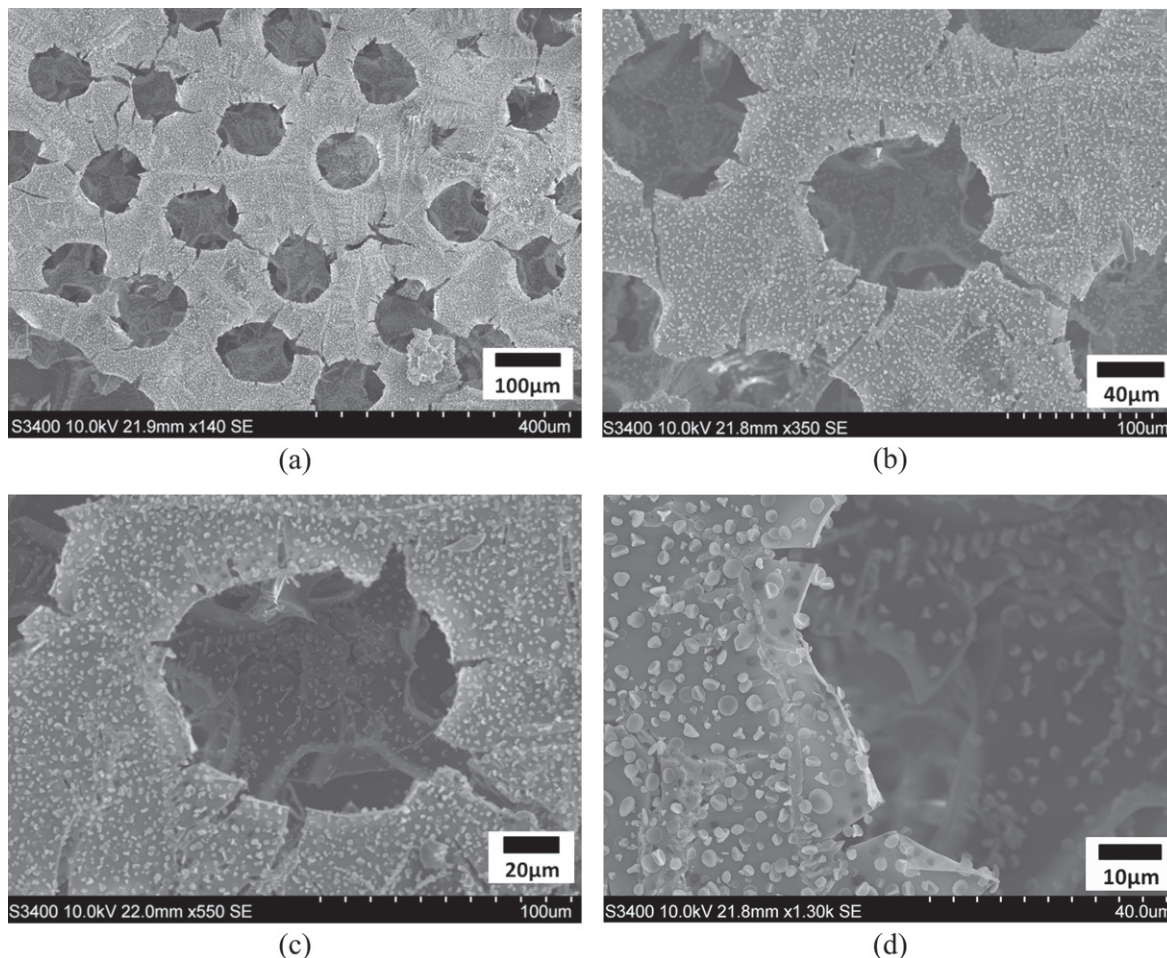


**Figure 8.** SEM images at different magnifications showing the same multilayered BSA scaffold after spraying with PMSQ micro-particles with images (a) and (d) having the lowest and the highest magnification, respectively.

### 3.4. Collagen beaded fibres spraying

Collagen beaded fibres with average fibre and bead sizes of  $257 \pm 25$  nm (mean diameter of 100 fibres) and  $685 \pm 67$  nm (mean diameter of 100 beads), respectively, were spun successfully onto the outer surface of the dried BSA scaffold, which had an average pore size of  $164 \pm 11$   $\mu\text{m}$ . Figure 10(a) shows SEM images at different magnifications of the same BSA scaffold after being sprayed with collagen beaded nanofibres for 5 min and figure 10(b) shows the same scaffold after spraying on it for 15 min. In this experiment it was not possible for the fibres to infiltrate into the inner structure of the scaffold due to their length. Although an attempt was made to spin the fibres simultaneously while the bubbles were produced from the T-Junction device, the bubble stability and self-assembly properties were affected thus causing the scaffold formation to fail.

## 4. Possible applications

The BSA scaffolds with secondary bio-products attached to them have potential applications in tissue and bone

regeneration engineering, wound care and cosmetics. BSA is a biocompatible and biodegradable FDA approved material that is non-toxic and can provide high cell affinity when the scaffold pore sizes are around 100–150  $\mu\text{m}$ [19]. In this study it was shown that the porosity of the scaffolds can be very easily controlled thus providing the necessary structure for different types of cell to achieve infiltration into the scaffold. The BSA solution can be replaced or combined with other materials such as hydroxyapatite that can be used for bone regeneration [40, 41]. The PLGA, PMSQ and collagen particles/fibres sprayed onto the scaffolds (which can also have a foam like texture) can be loaded with drugs, growth factors and other bioactive agents in order to achieve controlled release into locations such as wounds, thus accelerating the healing process and preventing infections [5, 42]. They can also be used in the cosmetic industry in the form of cream lathers and facial scrubbing creams to deliver vitamins, proteins and other substances into the skin [43]. The main advantage of using these biodegradable and biocompatible products produced in this work in cosmetics applications are that they are generally non-reactive when in contact with the human skin and by encapsulating them in

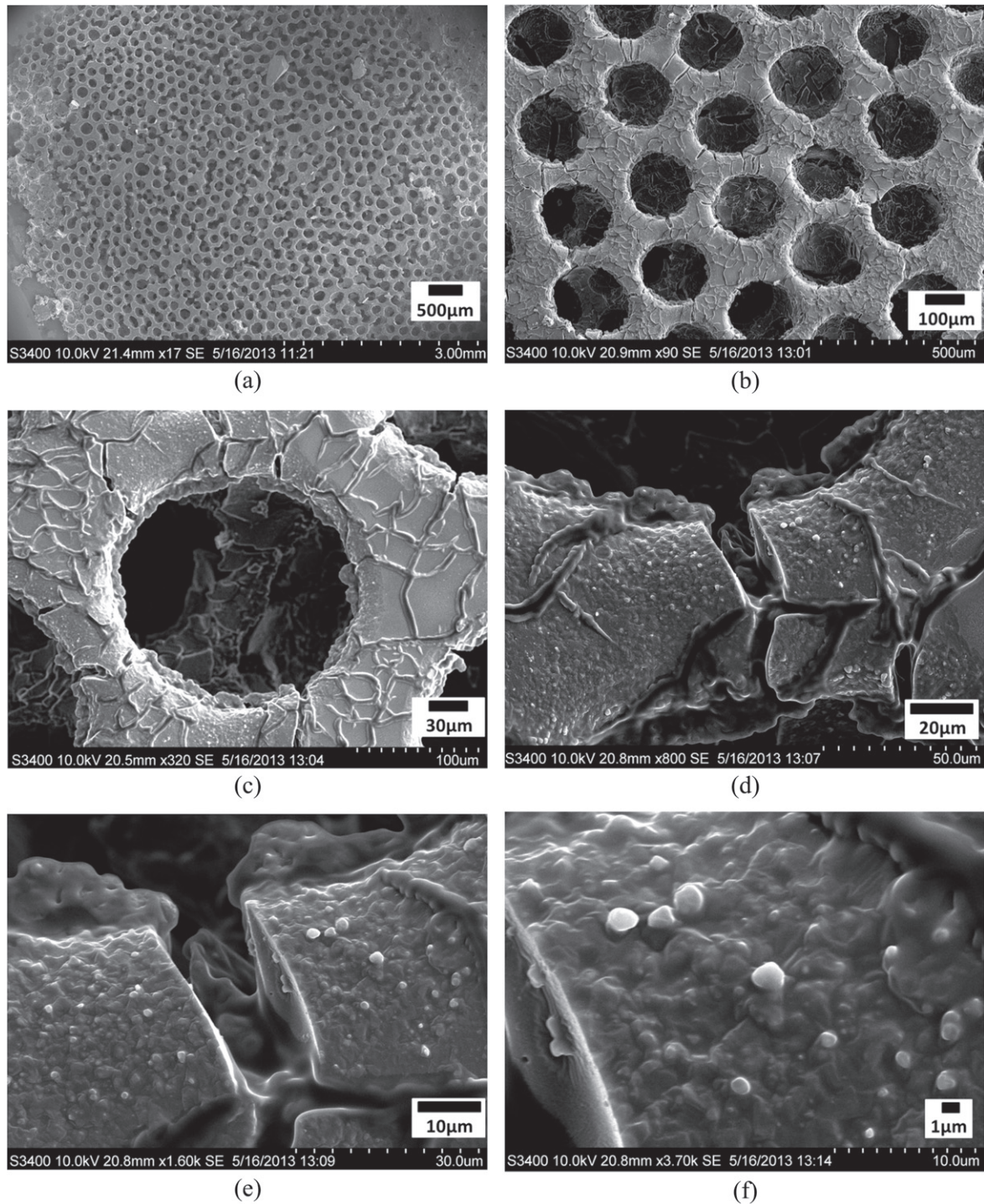


**Figure 9.** SEM images at different magnifications showing the same multilayered BSA scaffold after spraying with collagen micro-particles with images (a) and (f) having the lowest and the highest magnification, respectively.

the polymeric particles/fibres their biological stability can be increased [44].

## 5. Conclusions

In this study T-Junction microfluidic and EHD techniques were combined and used together successfully to engineer advanced biocompatible scaffolds containing secondary bio-

products in their structure. BSA protein scaffolds with controlled porosity varying from  $81 \pm 2 \mu\text{m}$  to  $543 \pm 33 \mu\text{m}$  were produced from microbubbles generated with the T-Junction technique by adjusting the operating parameters and solution properties. Once the microbubbles were dried, the 3D protein scaffold structures were obtained. The microbubbles produced with the T-Junction technique were highly mono-dispersed and hence led to the uniformity of the scaffold structure. Further by using the EHD process, biocompatible

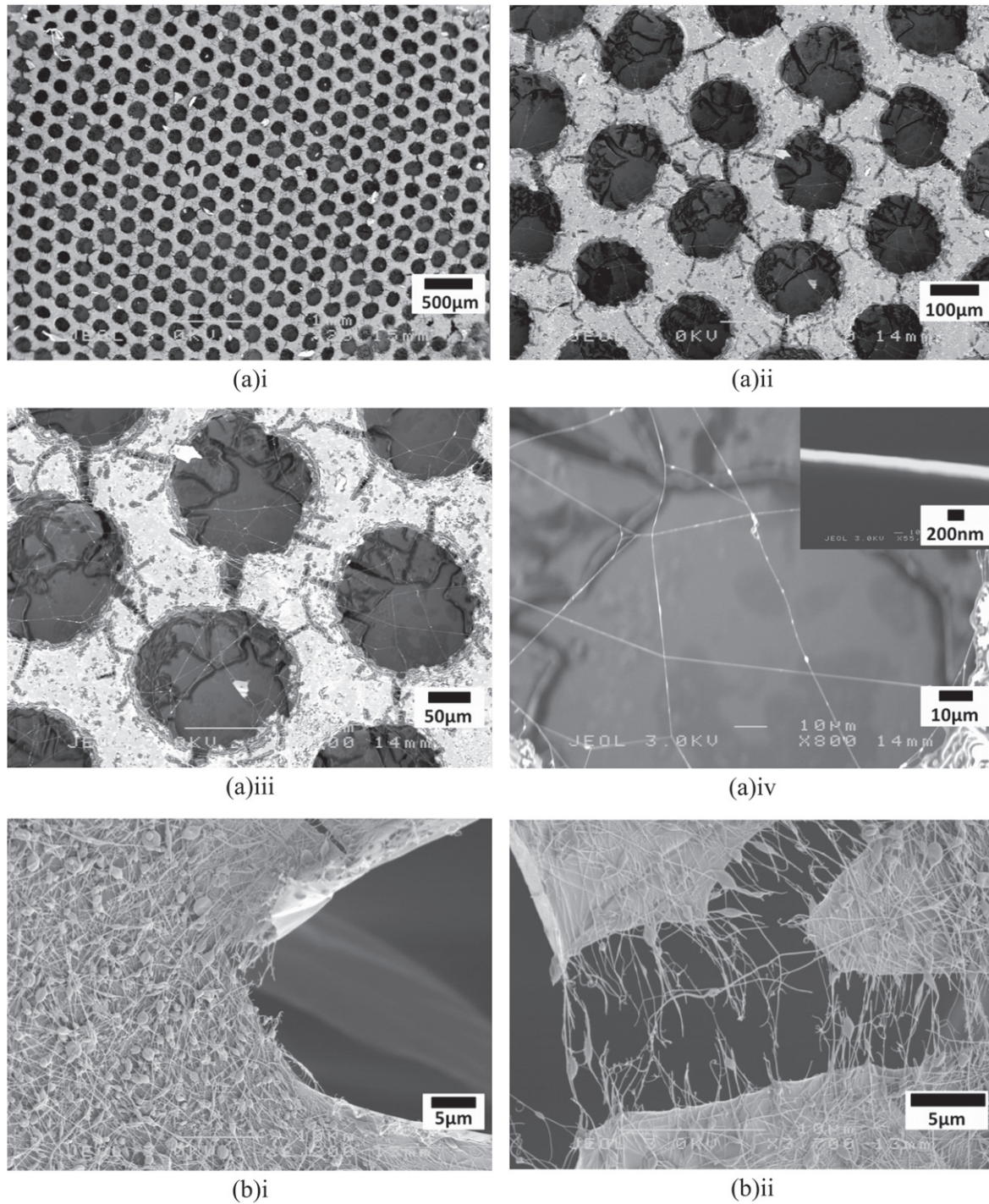


**Figure 10.** Scanning electron micrographs of multilayered BSA scaffolds sprayed with collagen beaded nanofibres for (a) 5 min and (b) 15 min at different magnifications.

PLGA, PMSQ and collagen particles having an average diameter of  $130 \pm 23$  nm,  $1.94 \pm 0.4$  µm and  $1.35 \pm 0.5$  µm, respectively, were produced and sprayed onto the scaffolds. Furthermore, beaded collagen nanofibres (fibre size:  $257 \pm 25$  nm and beads size:  $685 \pm 67$  nm) were spun on the BSA scaffolds. The BSA protein scaffolds with attached secondary bio-products formed in this work have the potential to be used as medical and tissue engineering scaffolds, as well as delivery devices containing multiple bioactive agents. It is

also believed that introducing these secondary elements in the scaffolds' assembly can improve with the mechanical strength of the structure.

**Acknowledgments**

The authors wish to thank the Engineering and Physical Science Research Council (UK) for providing the Phantom

V7.10 high speed camera for this work and the generous help of Adrian Walker of the EPSRC Engineering Instrument Loan Pool is gratefully acknowledged.

## References

- [1] Dhandayuthapani B, Yoshida Y, Maekawa T and Kumar D S 2011 Polymeric scaffolds in tissue engineering application: a review *Int. J. Polym. Sci.* **2011** 1–19
- [2] Cutroneo K R 2003 Gene therapy for tissue regeneration *J. Cellular Biochem.* **88** 418–25
- [3] Haynesworth S E, Reuben D and Caplan A I 1998 Cell-based tissue engineering therapies: the influence of whole body physiology *Adv. Drug Deliv. Rev.* **33** 3–14
- [4] Lee J-Y, Choi B, Wu B and Lee M 2013 Customized biomimetic scaffolds created by indirect three-dimensional printing for tissue engineering *Biofabrication* **5** 045003
- [5] Pereira R F, Barrias C C, Granja P L and Bartolo P J 2013 Advanced biofabrication strategies for skin regeneration and repair *Nanomedicine* **8** 603–21
- [6] Carletti E, Endogan T, Hasirci N, Hasirci V, Maniglio D, Motta A and Migliaresi C 2011 Microfabrication of PDLLA scaffolds *J. Tissue Eng. Regenerative Med.* **5** 569–77
- [7] Chan B P and Leong K W 2008 Scaffolding in tissue engineering: general approaches and tissue-specific considerations *Eur. Spine J.* **17** (Suppl. 4) 467–79
- [8] Hollister S J 2005 Porous scaffold design for tissue engineering *Nat. Mater.* **4** 518–24
- [9] Mikos A G, Thorsen A J, Czerwonka L A, Bao Y, Langer R, Winslow D N and Vacanti J P 1994 Preparation and characterization of poly(L-lactic acid) foams *Polymer* **35** 1068–77
- [10] Mallick K K 2009 Freeze casting of porous bioactive glass and bioceramics *J. Am. Ceram. Soc.* **92** S85–94
- [11] Liu J, Morykwas M J, Argenta L C and Wagner W D 2011 Development of a biodegradable foam for use in negative pressure wound therapy *J. Biomed. Mater. Res. B* **98B** 316–22
- [12] Sullivan A C and Jayasinghe S N 2007 Development of a direct three-dimensional biomicrofabrication concept based on electrospaying a custom made siloxane sol *Biomicrofluidics* **1** 034103–10
- [13] Li M Y, Mondrinos M J, Gandhi M R, Ko F K, Weiss A S and Lelkes P I 2005 Electrospun protein fibers as matrices for tissue engineering *Biomaterials* **26** 5999–6008
- [14] Xu T, Binder K W, Albanna M Z, Dice D, Zhao W, Yoo J J and Atala A 2013 Hybrid printing of mechanically and biologically improved constructs for cartilage tissue engineering applications *Biofabrication* **5** 015001
- [15] Lee K, Silva E A and Mooney D J 2011 Growth factor delivery-based tissue engineering: general approaches and a review of recent developments *J. R. Soc. Interface* **8** 153–70
- [16] Wang F, Guo G, Ma Q, Gu M, Wu X, Sheng S and Wang X 2013 Investigation on the thermo-mechanical properties and thermal stability of polylactic acid tissue engineering scaffold material *J. Therm. Anal. Calorimetry* **113** 1113–21
- [17] Kim H J, Kim U J, Vunjak-Novakovic G, Min B H and Kaplan D L 2005 Influence of macroporous protein scaffolds on bone tissue engineering from bone marrow stem cells *Biomaterials* **26** 4442–52
- [18] Nair A, Yang J and Tang L 2007 A Novel preparation of degradable scaffolds using BSA microbubbles as porogen *Engineering in Medicine and Biology Workshop, 2007* (Dallas: IEEE) pp 31–4
- [19] Nair A, Thevenot P, Dey J, Shen J, Sun M-W, Yang J and Tang L 2010 Novel polymeric scaffolds using protein microbubbles as porogen and growth factor carriers *Tissue Eng. C* **16** 23–32
- [20] Lima E G, Durney K M, Sirsi S R, Nover A B, Ateshian G A, Borden M A and Hung C T 2012 Microbubbles as biocompatible porogens for hydrogel scaffolds *Acta Biomaterialia* **8** 4334–41
- [21] Wang C-C, Yang K-C, Lin K-H, Liu H-C and Lin F-H 2011 A highly organized three-dimensional alginate scaffold for cartilage tissue engineering prepared by microfluidic technology *Biomaterials* **32** 7118–26
- [22] Chung K-y, Mishra N C, Wang C-C, Lin F-h and Lin K-h 2009 Fabricating scaffolds by microfluidics *Biomicrofluidics* **3** 022403–8
- [23] Chen C, Zhu Y, Leech P W and Manasseh R 2009 Production of monodispersed micron-sized bubbles at high rates in a microfluidic device *Appl. Phys. Lett.* **95** 144101
- [24] De Menech M, Garstecki P, Jousse F and Stone H A 2008 Transition from squeezing to dripping in a microfluidic T-shaped junction *J. Fluid. Mech.* **595** 141–61
- [25] Chiu P-J, Mei J-C, Huang Y-C and Yu J 2013 Monolayer microbubbles fabricated by microfluidic device for keratocytes observation *Microelectron. Eng.* **111** 277–84
- [26] Colosi C, Costantini M, Barbetta A, Pecci R, Bedini R and Dentini M 2013 Morphological comparison of PVA scaffolds obtained by gas foaming and microfluidic foaming techniques *Langmuir* **29** 82–91
- [27] Hu Y, Hollinger J O and Marra K G 2001 Controlled release from coated polymer microparticles embedded in tissue-engineered scaffolds *J. Drug Targeting* **9** 431–8
- [28] Enayati M, Ahmad Z, Stride E and Edirisinghe M 2009 Preparation of polymeric carriers for drug delivery with different shape and size using an electric jet *Current Pharm. Biotechnol.* **10** 600–8
- [29] Sofokleous P, Stride E and Edirisinghe M 2013 Preparation, characterization, and release of amoxicillin from electrospun fibrous wound dressing patches *Pharm. Res.* **30** 1926–38
- [30] Yoon H and Kim G 2011 A three-dimensional polycaprolactone scaffold combined with a drug delivery system consisting of electrospun nanofibers *J. Pharm. Sci.* **100** 424–30
- [31] Sofokleous P, Stride E, Bonfield W and Edirisinghe M 2013 Design, construction and performance of a portable handheld electrohydrodynamic multi-needle spray gun for biomedical applications *Mater. Sci. Eng. Mater. C* **33** 213–23
- [32] Sengupta D and Heilshorn S C 2010 Protein-engineered biomaterials: highly tunable tissue engineering scaffolds *Tissue Eng. B* **16** 285–93
- [33] Maas M, Bodnar P M, Hess U, Treccani L and Rezwani K 2013 Towards the synthesis of hydroxyapatite/protein scaffolds with controlled porosities: bulk and interfacial shear rheology of a hydroxyapatite suspension with protein additives *J. Colloid Interface Sci.* **407** 529–35
- [34] Ekemen Z, Chang H, Ahmad Z, Bayram C, Rong Z, Denkbas E B, Stride E, Vadgama P and Edirisinghe M 2011 Fabrication of biomaterials via controlled protein bubble generation and manipulation *Biomacromolecules* **12** 4291–300
- [35] Parhizkar M, Edirisinghe M and Stride E 2013 Effect of operating conditions and liquid physical properties on the size of monodisperse microbubbles produced in a capillary embedded T-junction device *Microfluid. Nanofluid.* **14** 797–808
- [36] Xie J and Wang C-H 2007 Encapsulation of proteins in biodegradable polymeric microparticles using electro-spray in the Taylor cone-jet mode *Biotechnol. Bioeng.* **97** 1278–90
- [37] Yarin A L, Koombhongse S and Reneker D H 2001 Taylor cone and jetting from liquid droplets in electrospinning of nanofibers *J. Appl. Phys.* **90** 4836–46
- [38] Danhier F, Ansorena E, Silva J M, Coco R, Le Breton A and Preat V 2012 PLGA-based nanoparticles: an overview of

- biomedical applications *J. Controlled Release* **161** 505–22
- [39] Yoon J-Y and Garrell R 2008 *Encyclopedia of Microfluidics and Nanofluidics* ed D Li (US: Springer) pp 68–76
- [40] Ishaug S L, Crane G M, Miller M J, Yasko A W, Yaszemski M J and Mikos A G 1997 Bone formation by three-dimensional stromal osteoblast culture in biodegradable polymer scaffolds *J. Biomed. Mater. Res.* **36** 17–28
- [41] Rathbone C R, Guda T, Singleton B M, Oh D S, Appleford M R, Ong J L and Wenke J C 2013 Effect of cell-seeded hydroxyapatite scaffolds on rabbit radius bone regeneration *J. Biomed. Mater. Res. A* **102** 1458–66
- [42] Boateng J S, Matthews K H, Stevens H N and Eccleston G M 2008 Wound healing dressings and drug delivery systems: a review *J. Pharm. Sci.* **97** 2892–923
- [43] Friess W 1998 Collagen–biomaterial for drug delivery *Eur. J. Pharm. Biopharm.* **45** 113–36
- [44] Ammala A 2013 Biodegradable polymers as encapsulation materials for cosmetics and personal care markets *Int. J. Cosmetic Sci.* **35** 113–24